Journal of Internal Medicine 2004; **256**: 205–223

KEY SYMPOSIUM

MRI and CSF studies in the early diagnosis of Alzheimer's disease

M. J. de LEON[1,2], S. DESANTI[1], R. ZINKOWSKI[3], P. D. MEHTA[4], D. PRATICO[5], S. SEGAL[1], C. CLARK[5], D. KERKMAN[3], J. DEBERNARDIS[3], J. LI[1], L. LAIR[1], B. REISBERG[1], W. TSUI[1,2] & H. RUSINEK[1]

From the [1]Center for Brain Health, New York University School of Medicine, NY; [2]Nathan Kline Institute, Orangeburg, NY; [3]Molecular Geriatrics, Vernon Hills, IL; [4]Institute for Basic Research, Staten Island, NY; and [5]University of Pennsylvania, PA, USA

Abstract. de Leon MJ, DeSanti S, Zinkowski R, Mehta PD, Pratico D, Segal S, Clark C, Kerkman D, DeBernardis J, Li J, Lair L, Reisberg B, Tsui W, Rusinek H. (New York University School of Medicine, NY; Nathan Kline Institute, NY; Molecular Geriatrics, Vernon Hills, IL; Institute for Basic Research, NY; and University of Pennsylvania, PA; USA). MRI and CSF studies in the early diagnosis of Alzheimer's disease (Key Symposium). *J Intern Med* 2004; **256**: 205–223.

The main goal of our studies has been to use MRI, FDG-PET, and CSF biomarkers to identify in cognitively normal elderly (NL) subjects and in patients with mild cognitive impairment (MCI), the earliest clinically detectable evidence for brain changes due to Alzheimer's disease (AD). A second goal has been to describe the cross-sectional and longitudinal interrelationships amongst anatomical, CSF and cognition measures in these patient groups. It is now well known that MRI-determined hippocampal atrophy predicts the conversion from MCI to AD. In our summarized studies, we show that the conversion of NL subjects to MCI can also be predicted by reduced entorhinal cortex (EC) glucose metabolism, and by the rate of medial temporal lobe atrophy as determined by a semi-automated regional boundary shift analysis (BSA-R). However, whilst atrophy rates are predictive under research conditions, they are not specific for AD and cannot be used as primary evidence for AD. Consequently, we will also review our effort to improve the diagnostic specificity by evaluating the use of CSF biomarkers and to evaluate their performance in combination with neuroimaging. Neuropathology studies of normal ageing and MCI identify the hippocampal formation as an early locus of neuronal damage, tau protein pathology, elevated isoprostane levels, and deposition of amyloid beta 1-42 (Aβ42). Many CSF studies of MCI and AD report elevated T-tau levels (a marker of neuronal damage) and reduced Aβ42 levels (possibly due to increased plaque sequestration). However, CSF T-tau and Aβ42 level elevations may not be specific to AD. Elevated isoprostane levels are also reported in AD and MCI but these too are not specific for AD. Importantly, it has been recently observed that CSF levels of P-tau, tau hyperphosphorylated at threonine 231 (P-tau231) are uniquely elevated in AD and elevations found in MCI are useful in predicting the conversion to AD. In our current MCI studies, we are examining the hypothesis that elevations in P-tau231 are accurate and specific indicators of AD-related changes in brain and cognition. In cross-section and longitudinally, our results show that evaluations of the P-tau231 level are highly correlated with reductions in the MRI hippocampal volume and by using CSF and MRI measures together one improves the separation of NL and MCI. The data suggests that by combining MRI and CSF measures, an early (sensitive) and more specific diagnosis of AD is at hand. Numerous

studies show that neither T-tau nor P-tauX (X refers to all hyper-phosphorylation site assays) levels are sensitive to the longitudinal progression of AD. The explanation for the failure to observe longitudinal changes is not known. One possibility is that brain-derived proteins are diluted in the CSF compartment. We recently used MRI to estimate ventricular CSF volume and demonstrated that an MRI-based adjustment for CSF volume dilution enables detection of a diagnostically useful longitudinal P-tau231 elevation. Curiously, our most recent data show that the CSF isoprostane level does show significant longitudinal elevations in MCI in the absence of dilution correction. In summary, we conclude that the combined use of MRI and CSF incrementally contributes to the early diagnosis of AD and to monitor the course of AD. The interim results also suggest that a panel of CSF biomarkers can provide measures both sensitive to longitudinal change as well as measures that lend specificity to the AD diagnosis.

Keywords: MCI, Alzheimer's disease, biomarkers, MRI, longitudinal, early diagnosis.

Introduction

The prevalence of Alzheimer's disease (AD) is expected to double over the next 30 years [1] and there is still no currently accepted early diagnosis for AD. As reported by the biomarkers in the AD working group of the Reagan Research Institute [2], with improved understandings of the pathophysiology of AD and the promises of mechanism-based and preventative therapeutic approaches, there is an urgent need to develop biomarkers for early diagnosis.

Magnetic resonance imaging (MRI) and CSF chemistry studies have been pointed to as candidate modalities for diagnostic biomarkers because they accurately diagnose AD, predict decline in mild cognitive impairment (MCI) patients, and in the case of serial MRI track the course of AD. Nevertheless, for several reasons these modalities are not widely accepted: (i) MRI tissue volume changes are not specific for AD and require intensive skilled labour; (ii) the pioneering CSF studies measured total T-tau level and CSF amyloid beta1-42 (Aβ42) which are not specific for AD, and do not readily change with disease progression; (iii) CSF Aβ42 levels are not easily interpreted because CSF Aβ is not exclusively brain-derived and because production and clearance are not well characterized; (iv) CSF acquisition is invasive; and (v) experimental amyloid imaging protocols are not clinically available nor adequately tested [3–8].

The neuropathology of early AD

The principal hallmarks of AD include: Aβ deposition in extracellular plaques and vascular walls, the accumulation of intracellular neurofibrillary tangles (NFT), synaptic reductions, neuronal loss and volume loss (atrophy)[9–12]. The hippocampal formation includes the EC, hippocampus proper, and subiculum, and it comprises the regions most vulnerable to the early deposition of AD lesions [12–19]. A pattern of hippocampal formation NFT deposition [20–29], with relative sparing of the neocortex [21–23, 25, 30], is often found in studies of nondemented elderly (this term includes both normal and MCI patients). Braak's neuropathology studies of 2369 cases demonstrated that in the most mildly affected brains, *only* the transentorhinal EC showed NFT and neuropil thread pathology [31]. These findings suggest that isolated NFT may first occur in the natural history of AD [24, 28, 32] but it does not exclude the possibility that soluble Aβ peptides are interactive [29, 33]. Of direct relevance to early diagnosis using neuroimaging, numerous pathology studies have shown that in mild AD there is damage to the hippocampal formation that includes synaptic loss (a site of active glucose metabolism), neuronal loss, volume reductions, and tau and Aβ pathology [18, 34–40]. It is well documented, that in AD hippocampal neuronal damage is reflected in volume losses that are detectable with MRI imaging [41, 42]. Of immediate importance to this application, studies by Price have shown that tau and Aβ pathology precede EC and hippocampal neuronal losses in nondemented and preclinical AD patients [43]. However, once the AD process is underway, it appears that the extent of hippocampal neuronal loss exceeds the number of NFT lesions [44]. Our pathology data [37, 38] is in

agreement with these observations and this leads to our main hypothesis: that baseline elevations of the CSF P-tau231 level and an elevated rate of MRI hippocampal formation atrophy will both within and combined across modalities optimize the prediction of longitudinal cognitive decline in normal elderly (NL) and in patients with MCI.

Compared with NFT, Aβ depositions tend to accumulate at greater ages. They too affect the hippocampal formation but have a preference for the neocortex [23–25]. Brain levels of both Aβ42 and Aβ40 are increased in MCI and AD [33]. Aβ42 aggregates more rapidly than Aβ40 and is the principal form deposited in plaques. Aβ40 is the predominant form found in vascular lesions and in the CSF. Recently, Thal *et al.* reported that Aβ plaque deposits begin in the temporal neocortex and then spread to involve the EC and hippocampus [45]. This appears to happen only after NFT pathology is established in those sites. The extent of the fibrillar Aβ burden has been associated, in early AD, with both cognitive impairment [46, 47] and dendritic damage [48]. Carriers of an apoE ε4 allele show at younger ages both increased EC NFTs [49] and neocortical Aβ deposits [50–52]. The evidence that early tangle and plaque pathology contributes to an increased risk for brain atrophy and cognitive decline, justified our longitudinal study of CSF biomarkers of these pathological features.

CSF tau studies

It is widely believed that increases in the CSF T-tau level reflect neuronal and axonal damage. Many studies demonstrate elevated CSF concentrations of T-tau in AD [53–64] and in MCI [54, 65, 66]. However, clinical studies show that elevated CSF T-tau levels are not specific to AD as they are elevated in other neurodegenerative diseases [67]. It was recently shown in acute stroke that the T-tau but not the P-tau levels were increased and later returned to normal [68]. One MCI study reported that T-tau alone was not an accurate baseline predictor of the decline to AD [65].

Moreover, considerable uncertainty exists with respect to the influence of ageing on the CSF T-tau levels. Normal ageing studies show both positive [69] and negative [53, 54] age effects. These studies are difficult to interpret due to the small numbers of subjects, narrow age distributions, diverse strategies for excluding cognitive impairment, and absent neuroimaging and autopsy validation.

It is very important that CSF prediction and differential diagnosis studies in MCI and AD consistently show that P-tau181 or P-tau231–235 [70, 71] or P-tau396/404 [72] are diagnostically equivalent or better than the T-tau. Predicting the conversion of MCI to AD, in the absence of controls, Arai *et al.* achieved equivalent accuracies from P-tau231–235 and T-tau levels [70]. However, Hampel *et al.* found in MCI that elevated levels of P-tau231 were superior to T-tau in the binary prediction of progressive cognitive decline to AD [73]. In a recent cross-sectional paper, Hampel's group reported that when compared with T-tau, P-tau231 showed significantly better specificity for AD [74]. Specifically, the levels of P-tau231, but not T-tau, were consistently elevated in AD when compared with frontotemporal dementia (FTD), lewy body dementia (LBD), and NL controls. Others have compared AD with FTD [71, 75] and with non-AD dementia controls [76, 77] and demonstrated a superior diagnostic specificity with P-tau181 relative to T-tau. Similarly, CSF P-tau396–404 but not T-tau differentiated AD ($n = 52$) from vascular dementia ($n = 46$) and NL ($n = 56$) (accuracy not reported) [72]. However, the ratio of P-tau396–404/T-tau differentiated the groups with a sensitivity and specificity greater than 95%. It was concluded that the major increase in X-tau detected in the CSF of AD is in the form of P-tauX.

Overall, these studies suggest that P-tau231 may provide unique and relatively specific diagnostic information for AD, whereas, T-tau may be a nonspecific marker for general brain damage [78]. To date, *in vivo* studies, have not examined any of the longitudinal relationships between MRI-determined EC, hippocampal, or neocortical volumes and CSF T-tau or P-tau231.

CSF Aβ studies

The genetic mutations causing familial AD elevate the production of Aβ, particularly Aβ42 [79]. However, there is little evidence for elevated CSF or plasma Aβ42 levels in sporadic AD. One study reported that the levels of Aβ42 are elevated in MCI and AD [80] but these results are not consistent [54]. Cross-sectional CSF Aβ studies consistently show that relative to normal control, Aβ42 levels

are reduced in AD [53, 81–85]. One longitudinal AD study showed that Aβ42 levels decreased over time [82]. Major obstacles to the interpretation of these CSF data include samples derived from multiple collaborating sites with potentially different thresholds for recognizing 'early' AD and the very limited availability of longitudinal data on normal individuals. The influences of normal ageing on CSF turnover and specifically on Aβ clearance are also poorly understood [86, 87]. It has been experimentally demonstrated that with increasing age, amyloid plaques start to accumulate in the brain and may act as a sink for soluble Aβ [88]. Based on this view, assuming production is constant, one would predict age-related plaque deposition with an associated decrease in the CSF Aβ level. However, if clearance were also reduced, then this potentially explains why cross-sectional studies show little evidence for a relationship between CSF Aβ42 and age [53, 54, 84]. Moreover, recent observations of reduced CSF Aβ levels in other dementias without plaque formation, alternatively, suggest that reduced neuronal production of Aβ is yet another variable. Evidence from transgenic AD-mice studies indicates that the relationships amongst brain, CSF and plasma levels change over time due to the progressive sequestration of Aβ42 in plaques. Nine-month-old AD mice with brain plaques showed a twofold higher CSF-to-plasma Aβ ratio than age and genetically matched animals without plaques [89].

The diagnostic utility of CSF Aβ40 as a biomarker is less well understood than Aβ42. A limited number of reports have shown elevated Aβ40 levels with increasing age [84, 90] and in MCI. However, several cross-sectional AD studies have failed to observe differences from NL [85, 91]. Longitudinal AD data for Aβ40 are limited and not consistent [82, 92]. It remains to be examined how well Aβ40 predicts the transitions between NL and MCI and between MCI and AD.

On the bright side, considerable agreement exists that in cross section, reduced CSF Aβ42 combined with elevated X-tau measures improves the diagnostic accuracy for AD [53, 54, 61, 62]. However, compared with non-AD dementia patients, Aβ42 reductions offer limited specificity for AD. Moreover, there is inadequate longitudinal data to make a judgement about the predictive value of Aβ4X for either future MCI or AD.

Physiological bases for stable CSF tau concentrations

Given the characteristic progressive clinical decline and increasing topography of brain atrophy in AD [93], it is surprising that CSF T-tau concentrations are not consistently found to be progressive. Whilst a few longitudinal AD studies report increases in T-tau levels [92, 94, 95], others do not show changes [65, 96–98]. Longitudinal AD levels of P-tau231 have not yet been reported. In a longitudinal MCI study using P-tau231–235, cross-sectional but not longitudinal level changes were found [70]. Speculative explanations for the negative longitudinal X-tau findings include the inadequacy of the follow-up interval and variability in the pathological course of AD. Our recent findings suggest that atrophy-related anatomical and physiological factors may also play a role [99]. We observed that only after controlling for the progressive ventricular enlargement in MCI and the resulting dilution of the CSF P-tau231 concentration were significant longitudinal level increases detected.

Our rationale for the ventricular volume correction is based on observations, that as a predominantly brain-derived protein, tau levels are higher in the ventricular than lumbar CSF. Reiber [100] has shown that the concentrations of brain-derived proteins are higher in ventricular than in lumbar samples (1.5 : 1 for tau and 18 : 1 for S-100B). For systemically derived proteins ratios <1 are found (e.g. albumin 1 : 205). Aβ levels are lower (1 : 2) in ventricular samples compared with LP-derived samples (K. Blennow, unpublished communication), likely reflecting the derivation of Aβ from both central and peripheral sources [101]. It is well known that AD patients show progressive enlargement of ventricular and subarachnoid compartments due to tissue loss. The increased fluid volume then dilutes the CSF concentration of brain-derived proteins (e.g. X-tau). AD patients also show reduced CSF turnover [102] which may stagnate and further increase ventricular CSF protein levels. Reiber has proposed that reduced CSF turnover would not only increase the ventricular concentration, but would also result in an increased concentration gradient for tau that would enhance transependymal clearance, leaving the lumbar CSF X-tau levels largely unchanged. However, empirical validation studies have not been carried out. Because of the diverse protein sources for Aβ, it is unknown how reduced

CSF turnover would affect the ventricular and lumbar levels. Overall, the available data suggest that in AD the X-tau concentration from an LP may underestimate the volume released from the brain. For CSF Aβ4X, ventricular levels are lower than lumbar levels and ventricular volume corrections are not warranted. In the studies below, we test the hypothesis that P-tau231 levels adjusted for ventricular volume improve the cross-sectional and longitudinal diagnostic classifications. Virtually nothing is known about cisternal and subarachnoid tau concentrations and therefore we did not correct for this CSF pool. In summary, it is generally accepted that lumbar CSF X-tau and Aβ4X concentrations are potentially useful surrogate markers of brain AD. However, the poor understanding of the physiological mechanisms governing protein production and clearance from brain [103] and accumulations in CSF and plasma may limit the clinical utility of the protein level. We propose that volume dilution studies of CSF X-tau are important first steps towards understanding the dynamics of this system.

CSF isoprostane levels

Whilst the precise cascade resulting in cell death in AD is unknown, recent studies have identified a role for oxidative stress and lipid peroxidation [104]. Isoprostane brain levels, by-products of lipid peroxidation are increased at post-mortem in AD [105, 106], and increased in cross-sectional *in vivo* CSF studies of both AD [106, 107] and MCI [108]. There are no longitudinal data available.

Neuroimaging and CSF biomarker studies

We could not find prior MCI or AD studies of the longitudinal relationships between neuroimaging measures and CSF measures of X-tau and/or Aβ4X levels. One encouraging prediction study of MCI and AD subjects reported that baseline CSF P-tau181 and Aβ42 levels predicted, at 16 months, ventricle volume increases [109].

Neuroimaging markers for MCI and AD

In 1989 we published the first study showing that qualitative estimates of hippocampal atrophy in MCI predicted decline to AD [110]. This finding has been replicated [111, 112] and more recently, predictions of future AD were demonstrated with hippocampal volume (see [113, 114] for review), and with hippocampal perfusion [115]. These early studies also demonstrated that the prevalence hippocampal atrophy increased with age and was very common in MCI and AD [116] (see Fig. 1).

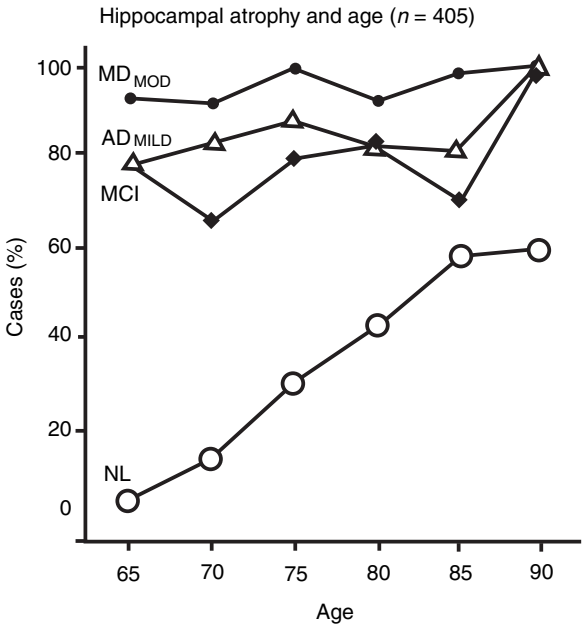

Fig. 1 Frequency of hippocampal atrophy as a function of age and diagnostic category.

Additional recent findings show that reduced EC size can discriminate between MCI and NL [117–122] and accurately predict future conversion of MCI subjects to AD [118, 122–124]. There is also evidence to show that size or glucose metabolism (METglu) in temporal neocortex [125–128] and posterior cingulate gyrus [115] can predict the MCI conversion to AD. However, the regional MRI brain volume or metabolism reductions determined by FDG-PET are not disease-specific. For example, both the EC and hippocampal volumes are reduced in AD and FTD when compared with control, and, these anatomical changes do not distinguish between the two disorders [129]. In addition, longitudinal whole-brain atrophy changes estimated from the boundary shift integral method fail to distinguish the abnormal rates of atrophic change characteristic of both AD and FTD [130, 131].

In 2001 using FDG-PET, we published the first evidence that EC METglu reductions in NL uniquely

predict the decline to MCI and also predict future hippocampal glucose metabolism reductions [124]. Our most recent MRI work shows that the medial temporal lobe atrophy rate during the normal stage, estimated with a boundary shift protocol, predicts the future conversion of NL to MCI [132]. Previously, Jack *et al.* demonstrated that NL patients who converted to MCI showed a greater rate of hippocampal volume loss than nondeclining subjects. However, baseline effects (prediction) were not observed [133]. Overall, these MRI/PET studies indicate the current potential of hippocampal formation atrophy measures to predict stage transitions related to AD as well as to describe disease progression from NL to MCI to AD levels of impairment. In our current research, we are now examining the added sensitivity and specificity that CSF biomarkers bring to the brain image in the early diagnosis of AD.

Methods

MRI image acquisition

Diagnostic evaluations. Fast spin-echo fluid-attenuated inversion-recovery (FLAIR) images (TR = 9000 ms, TE = 133 ms, 1 NEX, TI = 2200 ms, 3.3 mm slice thickness; 24 cm FOV) were obtained in 32 axial planes using a 256 × 192 acquisition matrix, with a 4-min acquisition time. The FLAIR sequence images the entire brain and is used to identify white matter lesions.

Research scan sequences. For the brain volume and the boundary shift analysis protocols, we used fast-gradient echo (FGE) images from a 3D coronal T1-weighted acquisition. Images are intensity normalized and baseline and follow-up scans are co-registered. This MRI protocol is remarkable for its high tissue contrast and good spatial resolution. The FGE sequence is defined as: TR 35 ms, TE 9 ms, 60° flip angle, 256 × 192 acquisition matrix, the section thickness is 1.7 mm which encompasses the entire brain without wrap artefact. We acquire 124 sections with a 24-cm FOV and 1 NEX for a total acquisition time of 12 min.

All quantitative work is blinded to all clinical data. File names are assigned sequential code numbers and image headers are stripped off demographic information. All images are transferred to our central image data bank and then to satellite Sun workstations for further processing. Image analysis is performed on a graphic workstation (Sun Microsystems, Santa Clara, CA, USA) using our locally developed MIDAS software running on a Unix operating system.

MRI image analysis

Qualitative assessments of hippocampal atrophy. Several years ago we demonstrated that both CT and MRI protocols could be used interchangeably to obtain sets of axial images parallel to the long axis of the hippocampus in order to evaluate the extent of hippocampal atrophy [116]. For both CT and T1-weighted MRI this consisted of contiguous 5 mm axial slices acquired at approximately 20° negative to the CM plane. For all study subjects, the hippocampus was examined for CSF accumulation in the regions of the transverse, choroidal and hippocampal fissures (see Fig. 2, arrow). The anatomical basis for this assessment is described in detail in a previous publication [111]. For each hemisphere, using previously published procedures, the extent of hippocampal atrophy was rated on a 4-point scale: (0 = none, 1 = questionable, 2 = mild/moderate and 3 = severe). A cut-off score of 2 or greater (definite CSF accumulation) on either hemisphere was considered evidence for qualitative hippocampal atrophy.

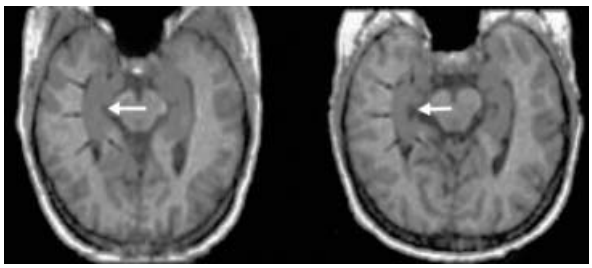

Fig. 2 Arrow highlights the body of the hippocampus. Image on right is from a patient with atrophy.

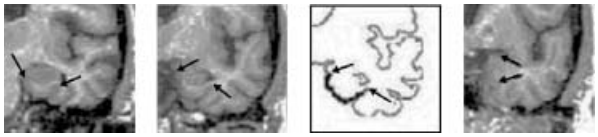

Fig. 3 Arrows mark the entorhinal cortex on MRI.

Quantitative assessments of regional brain size. EC. Measurement of the surface area of the EC requires drawings on the surface of the parahippocampal gyrus. In the coronal plane, the anterior limit of the EC is defined as 4 mm posterior to the 'fronto-temporal junction' (limen insulae). The posterior EC limit is demarcated by the anterior aspect of the lateral geniculate nucleus (LGN) defined by the recess of the LGN. Based on our validation study that used the FGE scan protocol, the lateral and medial EC boundaries are indicated by arrows in Fig. 3. The lateral (inferior) boundary of the EC in the more anterior sections is in the depth of the rhinal sulcus (panel C). In more posterior sections, the rhinal sulcus is often no longer recognizable, and the depth of the collateral sulcus is the lateral limit. This definition ensures the maximal inclusion of perirhinal and entorhinal cortex in the samples. For anterior levels, the medial EC boundary is in the sulcus semianularis between the convexities of the semilunar and ambient gyri. At more posterior levels with an uncal sulcus present, the medial limit is the uncus of the parahippocampal gyrus (panel B). This coincides with the grey matter found by extension of the white matter fibres of the angular bundle to the gyral surface (panel A). We measure on each coronal section the cortical ribbon from the medial to the lateral landmarks. The length is marked at the grey matter-CSF margin. The EC surface area is computed across slices.

Hippocampus.

In the human brain the hippocampus is well developed and occupies the floor of the temporal horn of the lateral ventricle. The length of the hippocampus is 4–5 cm, with a maximal width of about 2 cm and a maximal height of about 1.5 cm [134]. Our rules for the hippocampal volume have been validated at post-mortem, we have used them for many years, and they are similar to those of other investigators [135, 136]. Moreover, we have high levels of agreement between two raters (ICC = 0.94, $n = 16$). The full anterior hippocampus is measured. On coronal views, the hippocampus–amygdala boundary is difficult to distinguish. Using sagittal image reformats, where this boundary is readily apparent, we mark the boundary and transfer the markings to the coronal images. This technique has contributed to the high

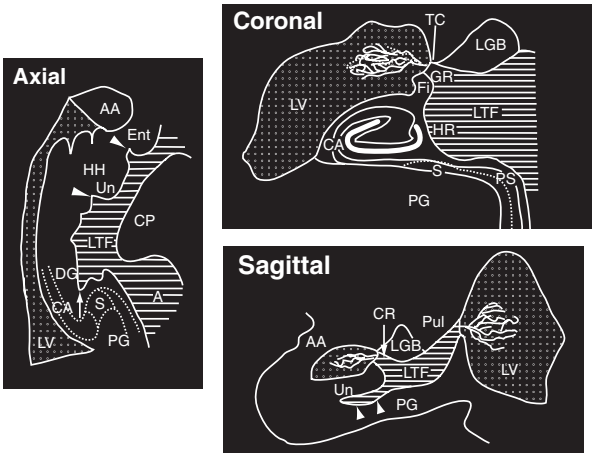

Fig. 4 The hippocampus viewed in tree orientations. HH, hippocampal head; AA, amygdala; Un, uncus; LTF, lateral transverse fissure; DG, dentate gyrus; LV, lateral ventricle; S, subiculum; A, ambient cistern; CP, pons; LGB, lateral geniculate body; PG, parahippocampal gyrus; Pul, pulvinar; TC, choroid plexus; Fi, fimbria; Ent, entorhinal cortex.

levels of agreement between two independent raters for amygdala volume measurements (ICC = 0.93, $n = 57$) [137]. In anterior hippocampal levels, the superior border is defined by the alveus and temporal horn of the lateral ventricle (LV, see Fig. 4). Laterally, the hippocampus is covered by the alveus and it sits under the floor of the temporal horn. The medial border of the anterior pes (uncal [UN]) hippocampus abuts the ambient cistern. The uncal sulcus [two arrows] separates the inferior surface of the pes hippocampus from the subiculum of the parahippocampal gyrus [PG]. At posterior levels, the smaller hippocampal body is bounded on its medial side by the lateral transverse fissure of Bichat [LTF] and the inferior boundary is the white matter of the parahippocampal gyrus. The superior boundary from lateral to medial is formed by the white matter of the temporal stem, tail of the caudate nucleus, lateral geniculate body [LGB] and pulvinar [PUL]. As the boundary between the CA1 of Ammon's horn and the subiculum [S] cannot be distinguished on MRI, we include subiculum in the hippocampal volume. The medial boundary of included subiculum is determined with reference to the superio-medial limit of the parahippocampal gyrus white matter. The most posterior limit of the hippocampus is the anterior crus of ascending fimbria-fornix.

Premorbid brain size correction.

To correct for head size variations across individuals we obtain an intracranial supratentorial volume using 2 mm thick sagittal images reformatted from the coronal FGE data [137, 138]. We trace the outline of the supratentorial compartment following the dural and tentorial surfaces on every third slice (mid-points every 6 mm). This estimate of premorbid brain size (prior to atrophy) is needed to statistically control for the relationship between regional volumes and brain size.

Regional boundary shift analysis.

Using this semi-automated protocol, relative atrophy in several 3D rectangular solids, size scaled by reference to x, y and z brain dimensions, are evaluated. The primary region examined was the MTL. The MTL region is centred over the hippocampus body (see Fig. 7 below) at the lateral geniculate level and extends both anteriorly to the amygdala to include pes hippocampi and posteriorly to the hippocampal tail to the level of the crus of the fornix [132].

Neuropsychological evaluations

A standard neuropsychological test battery was routinely administered to all subjects. The battery was developed to assess cognitive abilities that change with age, MCI and AD. The measures include the Guild Memory Test (Guild) [139], the Wechsler Memory Scale- Revised (WMS-R) [140], the NYU Computer Battery [141] and other supplemental tests. Multiple versions for many of these tests are routinely and systematically used over successive follow-ups.

Lumbar puncture and CSF collection

Patients arrived at the radiology suite at 9 AM after overnight fasting (12 h). A 15-cm^3 volume of clear CSF is collected into three polypropylene tubes using a fine LP needle guided by fluoroscopy. Just prior to the LP, 35 cm^3 of blood is collected. All CSF samples are kept on ice for a maximum of 1 h until centrifuged for 10 min at 450 ***g*** at 4 °C; 0.25 mL aliquots of the extracted plasma and CSF are stored in polypropylene tubes at −80 °C. After the LP, all patients are expected to rest for 2–3 h (to avoid headache).

CSF phospho-tau 231. CSF P-tau231 measurements were determined by Applied Neurosolutions (Vernon Hills, IL, USA) with a sandwich ELISA that detects tau phosphorylated at threonine 231 (P-tau231) in CSF. In this assay, tau is captured with two backbone-directed antibodies, tau-1 and CP-27. The captured tau is then detected by CP9, which is specific for P-tau231. The standard used in this assay is full-length recombinant human tau (441 aa) which is phosphorylated using a neuroblastoma cell extract in the presence of an ATP regeneration system. Additionally, the recombinant tau is reduced to a monomeric form to mimic the phospho-tau found in human CSF. The detection limits for these assays are 60 pg mL^{-1} for total tau (INNOTEST hTau) and 9 pg mL^{-1} for P-tau231 (MGC assay). The coefficients of variability for both assays ranged 5.5–11% (intra-assay) and 11.6–13.6% (inter-assay). Blind to clinical groups, we measure levels of T-tau and P-tau231 in batch mode.

CSF amyloid beta assays. Aβ 40 and Aβ42 ELISA. Plasma and CSF Aβ levels are blindly measured using monoclonal antibody 6E10 (specific to an epitope present on Aβ-16) and rabbit antisera to Aβ 40 and AB42, respectively, in a double antibody sandwich ELISA [85, 142]. The detection limit for Aβ40 and AB42 was 10 pg mL^{-1}. The coefficients of variability ranged 8–14% (intra-assay) and 10–18% (inter-assay).

CSF levels of rabbit antisera to CSF Aβ40 and Aβ42. Aβ32-40 and Aβ33-42 peptides synthesized commercially (Ana Spec, San Jose, CA, USA) were conjugated to keyhole limpet haemocyanin in PBS with 0.5% glutaraldehyde. Rabbits were immunized with the peptides and the specificity of antisera was examined in a sandwich ELISA. There was a strong response of rabbit antiserum to Aβ40 with 1 ng mL^{-1} of Aβ40 but there was no detectable response with 10 ng mL^{-1} of Aβ42. Similarly, antiserum to Aβ42 showed strong response with 1 ng mL^{-1} of Aβ42 but showed no reaction with 10 ng mL^{-1} of Aβ40. Western blot also showed that antiserum to Aβ40 was specific for Aβ40 and antiserum to Aβ42 was specific for Aβ42 [143]. Blind to clinical groups, the

levels of Aβ40 and Aβ42 in batch mode were measured.

Isoprostane (8,12-iso-iPF2a-VI). CSF samples were spiked with a fixed amount of internal standard (d_4−8,12-*iso*-$iPF_{2\alpha}$-VI) and extracted on a C18 cartridge column. The eluate was purified by thin-layer chromatography and finally assayed by negative ion chemical ionization gas chromatography/mass spectrometry [107]. The coefficient of variation ranged 4–7% (intra-assay) and 4.5–6.5% (inter-assay). Blind to clinical groups, the isoprostane levels in batch mode were measured.

Results

Hippocampal size, a marker in MCI for future AD

For 15 years, we have studied longitudinal and post-mortem hippocampal imaging in normal (NL) ageing, MCI, AD and normal pressure hydrocephalus [110, 111, 116, 144–149]. In our early studies using qualitative techniques, we were the first to show that the hippocampal size reduction is found in MCI is a predictor of future AD [110, 111]. In more recent cross-sectional and prediction studies, logistic regression analyses showed that hippocampal volume was the only anatomical measurement to significantly classify MCI and elderly NL controls [150, 151]. When contrasting MCI and AD patients, inclusion of the fusiform gyrus volume in the model significantly improved the ability of the hippocampal volume to separate the groups [125]. These data provide strong evidence that AD-related volume losses are most readily detected in the hippocampus in MCI, and indicate that in predicting the transition to dementia, it is important to consider both hippocampal and lateral temporal lobe volume reductions.

Hippocampal size and declarative memory performance

In our cross-sectional studies of NL and MCI, when compared with a temporal lobe neocortical reference volume, the hippocampal volume showed an anatomically unique correlation to delayed verbal recall [150, 152]. In a 4-year follow-up study of 44 NL subjects, we observed that reduced delayed recall performance was predicted by a smaller baseline hippocampus [153] ($R^2 = 0.65$, $P < 0.001$). However, the diagnostic accuracy of the hippocampus to predict progressive memory decline was poor (sensitivity 63% and specificity 80%). Overall, these data suggested that the hippocampal volume was more useful in predicting decline at the MCI stage than at a stage of normal cognition. These studies led to the development of the EC work (below).

Neuropathological validation studies of the MRI hippocampal volume

We recently completed a neuropathological validation study of the MRI hippocampal volume [42]. Specifically, the hippocampal volumes from 16 AD and four NL were determined from hemispheric tissue sections and from comparably sliced post-mortem T1-weighted MRI scans. We made unbiased estimates of the number of hippocampal neurons. There was a strong correlation between the MRI and the histological-derived hippocampal volumes ($r = 0.97$, $P < 0.001$). Restricting the analysis to the AD group left the correlation unchanged ($r = 0.97$, $P < 0.001$). The difference in the hippocampal volumes between normal and AD groups was 42% for the MRI data, and 40% for the histology data after adjusting for tissue shrinkage during specimen processing. Moreover, both the histology-based and the MRI based hippocampal volume measurements were significantly associated with the number of hippocampal neurones, ($r = 0.91$, $P < 0.001$ and $r = 0.90$, $P < 0.01$, respectively, see Fig. 5).

EC glucose metabolism predicts conversion from NL to MCI

In a longitudinal FDG-PET study of NL (mean age = 72 years, range 60–80 years), the EC volume was precisely defined on MRI using our published criteria [121] and used to sample the co-registered PET scan. We reported [124] that only baseline EC METglu reductions accurately predicted decline to MCI (sensitivity 83%, $n = 12$, specificity 85%, $n = 13$), [χ^2 (1) = 20.8, $P < 0.001$, odds ratio = 1.42, 95% CI = 1.08–1.88]. Those NL subjects who progressed to MCI also had, at follow-up, metabolism reductions in the EC, hippocampus and temporal neocortex. These FDG-PET data further support the value of the EC and hippocampus examinations in the characterization of the earliest brain changes associated with cognitive decline.

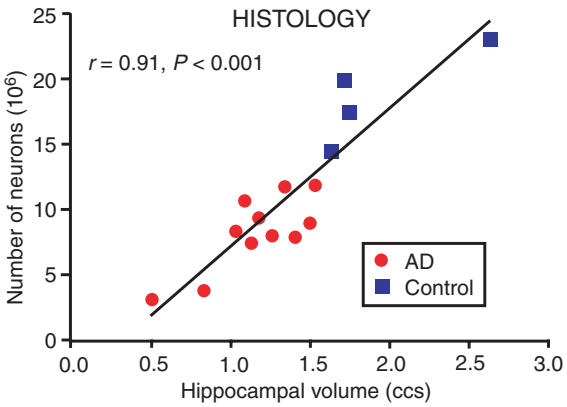

Fig. 5 The relationship between the total number of neurones in the hippocampus as a function of the hippocampal volume.

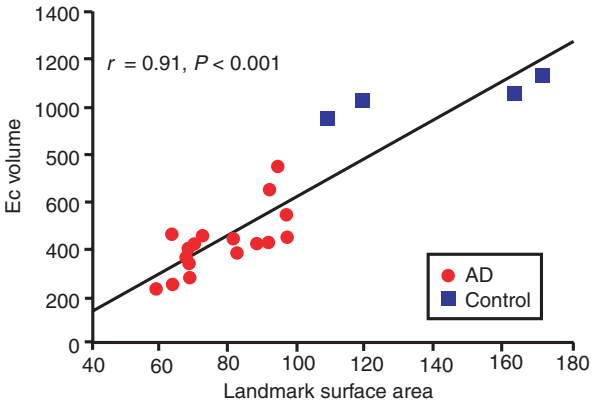

Fig. 6 The relationship between the histological definition of entorhinal cortex volume and the surface area of the entorhinal cortex using landmarks that can be recognized on MRI.

Neuropathological validation studies of the MRI entorhinal cortex surface area

We recently published the validation for the MRI measurement of the surface area of the EC [121]. The grey and white matter boundaries of the entorhinal and perirhinal cortices (EC) are poorly demarcated on MRI making cortical ribbon volume studies unreliable with standard MRI imaging protocols. Using post-mortem materials we validated an MRI image analysis method that avoids this problem by estimating the surface area of the EC (the sum across slices of the ribbon lengths multiplied by the slice thickness). We used serial 3 mm sections stained with cresyl violet to define three measurements: a histology-based EC volume, a histology-determined EC surface area, and EC surface area based on sulcal and gyral landmarks visible on MRI (EC-MRI). We studied 16 AD patients and four NL controls. The histology surface area was measured between the most medial boundary (pyriform cortex, or amygdala, or presubiculum, or parasubiculum) and the most lateral aspect (alternatively referred to as perirhinal, transentorhinal cortex, or Brodman's area 35). Using the MRI landmark method, the surface area was bounded medially (superiorly) by the sulcus semianularis on anterior sections and the medial parahippocampal gyrus on posterior sections. The lateral (inferior) boundary, in the anterior sections was the depth of the rhinal sulcus and in the posterior sections, the depth of the collateral sulcus. The results showed that the volume of the EC was significantly related to both surface area measurements (histological $r = 0.94$, $P < 0.001$, and landmark $r = 0.91$, $P < 0.001$; see Fig. 6). Between the two groups, the following measures were significantly ($P < 0.01$) reduced in AD: volume 61%, histological surface area 49% and landmark surface area 45% (see appendix). In addition, an *in vivo* study of eight NL and eight mildly impaired AD patients was included in this publication. Significant between group differences of 27% were observed for the landmark EC method and 12% differences for the hippocampal volume. Individually, the EC correctly classified 100% of the controls and 87% of the AD group. By comparison, the hippocampus classified 88% of the controls and 75% of the AD patients. Multivariate logistic regression models showed that the EC was superior to the hippocampus in the diagnostic classification of the groups [χ^2 (1) = 22.2, $P < 0.001$]. The landmark technique will be used in the proposed work.

Semi-automated medial temporal lobe atrophy predicts the conversion from NL to MCI

Forty-five NL elderly subjects were given a comprehensive battery of clinical and neuropsychological tests at baseline and at three follow-ups (2, 4 and 6 years [132] (see Table 1). Serial imaging was acquired twice with the same GE 1.5T MRI machine, at baseline and after 2 years. Brain atrophy rate was assessed using an automated procedure following the Boundary-Shift Algorithm (BSA) approach of Fox [154, 155]. Volumetric analyses were restricted to 3-D boxes that were applied to the baseline and the follow-up scans (Fig. 7). The MRI signal inten-

Table 1 Study subject ($n = 45$) grouping by clinical outcome

	NL → NL ($n = 32$)	NL → MCI ($n = 13$)	P*
Gender (male/female)	12/20	8/5	0.19
Education (years)	15.7 ± 5.1	14.9 ± 1.9	0.32
Age (years)	68.2 ± 5.1	73.6 ± 4.1	0.002
APOE type (E4+/E4−)	7/25	3/9	0.33
GDS (baseline)	1.9 ± 0.4	2.0 ± 0.0	0.10
GDS (year 2)	2.1 ± 0.5	3.2 ± 0.9	0.001
MMSE (baseline)	29.2 ± 1.1	29.0 ± 0.8	0.59
MMSE (year 2)	29.0 ± 1.2	27.1 ± 2.5	0.02
Years between scans	2.2 ± 0.4	2.3 ± 1.1	0.49
Years to last examination	6.3 ± 1.0	5.3 ± 2.4	0.15

*Proportions were examined using Fisher's exact test. *t*-Tests were used for comparison of mean values.

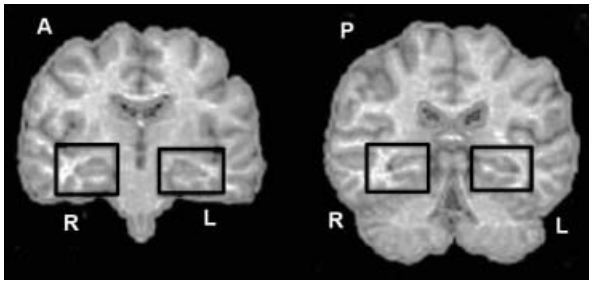

Fig. 7 Overall head-size adjusted boxes placed over the hippocampal region to facilitate the automated calculation of atrophy change using the regional boundary shift technique.

sity in the regions was normalized using regional (r) brain signal averages and converted to the brain volume using the partial volume decomposition method [156]. The BSA-r volume conversion assumes a fixed average contrast (3.13 : 1) between the brain parenchyma and the CSF as determined by a phantom study with our T1-weighted imaging sequence.

The atrophy at baseline and follow-up was defined as the ratio of the CSF volume to the total ROI volume. The annual percentage atrophy rate in each ROI was expressed as follow-up minus the baseline brain volume, divided by the baseline volume and by the time between the two MRI scans. In this study we examined the averaged right and left medial temporal lobe regions and a large region encompassing most of the brain. At the 2 year time point, seven of the 45 subjects showed objective evidence of cognitive decline. By the 6 year time point, a total of 13 had declined. The results in Table 2 show that both baseline and 2 year annualized rates of change for the MTL separated the declining and nondeclining NL groups. At baseline and at follow-up, whole brain atrophy was also increased in the decliners, but this measure did not show longitudinal progression. Of particular interest, the NL group that declined to MCI several years after the second scan ($n = 6$) also showed a significantly elevated MTL atrophy rate (0.7% per year) when compared with the 32 nondeclining NL group (0.3% per year; $t(36) = -3.1$, $P < 0.01$).

Table 2 Distribution of cross-sectional and longitudinal atrophy

	NL → NL ($n = 32$)	NL → MCI ($n = 13$)	P*
Whole brain % CSF (baseline)	20.4 ± 1.6	22.1 ± 1.4	0.001
Whole brain % CSF (year 2)	21.4 ± 1.8	23.9 ± 1.6	0.0001
MTL % CSF (baseline)	18.0 ± 3.5	21.5 ± 3.2	0.004
MTL % CSF (year 2)	18.4 ± 3.7	23.1 ± 3.3	0.0003
Whole brain annual atrophy rate	0.6 ± 0.4	1.3 ± 1.6	0.14
MTL annual atrophy rate	0.3 ± 0.4	0.9 ± 0.3	0.0001

*Tests for group differences were carried out using *t*-test.

After controlling for age, gender, education and the rate of whole brain atrophy, a forward stepwise logistic regression identified the MTL atrophy rate as a significant predictor of decline for both the total group of decliners and those that declined after the second MRI. The overall accuracy of MTL prediction was 89% (40/45), with 94% specificity (30/32) and 77% sensitivity (10/13). The odds ratio for cognitive decline was 1.7 (95% confidence interval 1.2–2.3) for each 0.1% of MTL atrophy rate as a risk factor. The model did not reach significance with entry of the whole brain atrophy rate in the last position. The results of this MRI prediction study demonstrate the importance of serial MTL imaging in monitoring the early course of memory decline.

CSF and MRI biomarkers

In a 1-year follow-up study of NL elderly ($n = 10$, GDS = 1.6 ± 0.5, MMSE = 29.4 ± 0.7, age = 62.5 ± 9.2) and MCI ($n = 8$, GDS = 3.0 ± 0.4, MMSE = 28.5 ± 1.2, age = 69.8 ± 9.2) we examined lumbar CSF levels (pg mL^{-1}) of P-tau231, Aβ40, Aβ42 and isoprostane. At baseline, follow-up and longitudinally, we compared the MCI group and the NL control group. During the study, one MCI patient converted to AD.

Table 3 Diagnostic specificity and accuracy for significant univariate and combinations of cognitive, MRI and CSF measures (sensitivity ≥ 75%)

Logistic regression model	Results at last step		
	Specificity (%)	Overall accuracy (%)	*P*
Baseline			
HIP volume	80	78	≤0.01
P-tau 231 level	80	78	≤0.05
P-tau 231 load	70	78	≤0.05
Isoprostane	90	89	≤0.001
Aβ40	100	89	≤0.01
Paragraph immediate recall	90	89	≤0.01
Paragraph delayed recall	90	83	≤0.001
Longitudinal			
P-tau 231 level	50	61	≤0.05
P-tau 231 load	90	83	≤0.01
Isoprostane	90	89	≤0.05

CSF protein levels. P-tau 231. P-tau231 levels were elevated in the MCI group at baseline ($U = 14.0$, $P \leq 0.05$, $n = 18$) and at follow-up ($U = 6.0$, $P \leq 0.01$, $n = 18$). This resulted in an overall classification accuracy of 78% at baseline [χ^2 (1) = 5.2, $P \leq 0.05$, see Table 3]. In the longitudinal analysis, a small but significant change was observed.

Amyloid beta. CSF Aβ40 levels were elevated in the MCI group at baseline ($U = 13.0$, $P \leq 0.05$, $n = 18$) and follow-up ($U = 17.0$, $P \leq 0.05$, $n = 18$). This resulted in an overall classification accuracy of 89% at baseline [χ^2 (1) = 7.1, $P \leq 0.01$]. After controlling for age, Aβ40 lost the baseline effect ($P < 0.05$) and kept the follow-up effect ($U = 17$, $P < 0.05$, $n = 18$). Aβ42 levels did not differ between the two groups at baseline. No longitudinal effects were observed for either Aβ40 or Aβ42.

Isoprostane. Isoprostane levels were elevated at both baseline ($U = 3.0$, $P \leq 0.001$, $n = 18$) and follow-up ($U = 6.0$, $P = 0.001$, $n = 18$). This resulted in an overall classification accuracy of 83% at baseline [χ^2 (1) = 15.9, $P \leq 0.001$]. After controlling for age, there was little change in the results. Moreover, a significant longitudinal change was seen in the MCI patients relative to control ($U = 15.0$, $P \leq 0.05$, $n = 18$). This resulted in an overall classification accuracy of 89% for the delta [χ^2 (1) = 4.0, $P \leq 0.05$]. The post hoc examination showed a significant isoprostane increase restricted to the MCI group (Wilcoxon signed ranks test $Z = -2.38$, $P \leq 0.05$, $n = 18$).

MRI volume data. Hippocampal volume. The hippocampal volume ratio was reduced in MCI by 19% at baseline [$t(16) = 3.4$, $P \leq 0.01$] and by 21% at follow-up [$t(16) = 3.5$, $P \leq 0.01$]. This resulted in an overall classification accuracy of 78% at baseline [χ^2 (1) = 9.3, $P \leq 0.01$]. After controlling for age, there was little change in the results. No longitudinal hippocampal volume change was observed.

Dilution correction-protein load. To correct for the dilution of tau in the ventricular compartment, typically enlarged in AD (see central white area of Fig. 8) we estimated ventricular CSF P-tau231 load (ng) by multiplying the P-tau231 level (pg mL^{-1}) by the ventricular volume (mL) and dividing by 1000 [99]. P-tau231 loads were elevated in the MCI group at baseline (Mann Whitney $U = 11$, $P < 0.01$, $n = 18$) and at follow-up ($U = 6$, $P = 0.001$, $n = 18$, see Table 4). In the longitudinal design, we observed a significant group by time interaction for the annualized P-tau231 load ($U = 12.0$, $P < 0.05$, $n = 18$). Follow-up examination showed a significant P-tau231 load increase in the MCI group (Wilcoxon signed ranks test $Z = -2.1$, $P < 0.05$, $n = 8$). No longitudinal load effects were observed for the controls.

We directly compared annualized longitudinal P-tau231 load and P-tau231 level changes, using two logistic regression models with reversed orders of entry, in the prediction of diagnostic group. At the first entry steps, both ΔP-tau231 level and ΔP-tau231 load significantly predicted group membership [$\chi^2(1) = 4.45$, $P \leq 0.05$ and $\chi^2(1) = 9.08$, $P \leq 0.01$ respectively. Comparing the second entry steps, the ΔP-tau231 load uniquely increased the variance explained by the ΔP-tau231 level [R^2 change = 0.23, $F(1,15) = 5.8$, $P \leq 0.05$].

Longitudinal correlation in MCI of AD-related CSF proteins with hippocampal volume

Because of the known inverse relationships at postmortem between the hippocampal volume and tau pathology and between brain Aβ42 load and hippocampal volume reductions, we examined the hypothesis that these relationships could be inferred *in vivo* using MRI and CSF. At baseline, for the entire

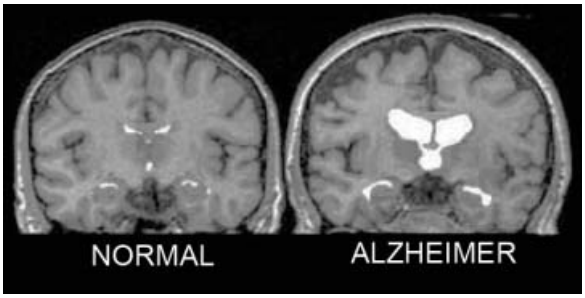

Fig. 8 Ventricular anatomy highlighted in a control and in an AD patient.

sample ($n = 18$), a significant inverse relationship was found between the hippocampus volume and the P-tau231 level ($r = -0.47$, $P < 0.05$). After controlling for age, there was little change in the results. In the 2 time-point longitudinal design, the MCI group, $n = 8$, showed a strong inverse relationship between hippocampal volume reductions and elevations in P-tau231 level ($r = -0.80$, $P < 0.05$, Fig. 9a). Also for MCI, the reduction in CSF Aβ42 levels showed a strong positive relationship to the reduction in the hippocampal volume ($r = 0.75$, $P < 0.05$, Fig. 9b). Moreover, in the MCI group the longitudinal changes in Aβ42 and P-tau231 showed a trend for the expected inverse relationship ($r = -0.56$, $P = 0.07$, one-tail).

Conclusions

Both neuropathology and neuroimaging studies converge on observations that hippocampal formation pathology is an early feature of AD. Over the past 15 years, numerous studies have identified hippocampal atrophy as a predictor of the decline from MCI to AD. It also appears that the EC of the hippocampal formation has value potentially as an even earlier marker of brain AD. Specifically, EC changes may actually precede hippocampal changes in NL at risk for future MCI. Additional work is required to better understand the temporal relationships between EC and hippocampal changes as well as the optimal image acquisition and image measurement strategies to use. Nevertheless, solely imaging the structural defects or the patterns of glucose metabolism reductions are not likely to be diagnostically specific indicators for AD. Recent studies show that neither the hippocampal atrophy nor its longitudinal rate of change are useful in

Table 4 Baseline and follow-up MRI and CSF measures (mean ± SD, group % differences and *P*)

	Baseline			Follow-up		
Measure	NL	MCI	% Diff	NL	MCI	% Diff
VV (cm^3)	29.7 ± 9.8	42.3 ± 15.2	42[a]	32.6 ± 10.3	45.7 ± 14.6	40[b]
P-tau231 level (pg mL^{-1})	160.0 ± 190.4	534.7 ± 451.8	234[a]	111.4 ± 158.0	563.9 ± 478.0	406[b]
P-tau231 load (ng)	5.6 ± 9.1	19.7 ± 15.3	252[b]	4.7 ± 8.6	22.8 ± 17.5	385[b+]
Aβ40 level (pg mL^{-1})	9596 ± 2317	12393 ± 2389	29[a]	8825 ± 2145	11876 ± 2909	35[a]
Aβ42 level (pg mL^{-1})	1015.1 ± 448.3	943.7 ± 486.7	−7	1040.3 ± 413.2	903.7 ± 484.1	−13
IP level (pg mL^{-1})	28.0 ± 6.36	47.9 ± 11.3	71[b]	33.4 ± 15.0	66.5 ± 25.9	99[b+]

VV, ventricle volume; load = ng, IP = isoprostane; % Diff, cross-sectional differences: (MCI−NL)/NL. Cross-sectional effects: [a]$P \le 0.05$; [b]$P \le 0.01$. Annualized longitudinal effects: + = $P \le 0.05$.

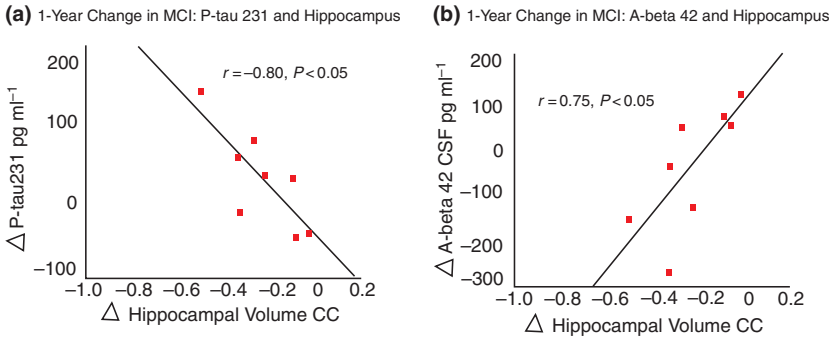

Fig. 9 Relationships between longitudinal changes in hippocampal volume and changes in CSF levels of (a) P-tau231 and (b) amyloid beta 1-42.

separating fronto-temporal dementia from AD. CSF P-tau231in combination with Aβ4X studies offers the promise of a specific *in vivo* diagnosis of AD. By combining MRI and CSF measures, the preliminary results suggest that both an early sensitive and specific diagnosis for AD is a possibility. Studies by Hampel suggest that elevated P-tau231 measurements may be specific for AD and this important observation requires replication as well as extension to MCI.

In the MCI stage of AD, both the hippocampal volume and the CSF P-tau231 concentration predict future AD. However, the magnitude of the agreement between these predictors of conversion has not been reported. Our preliminary data suggest that they are related and potential indicators of a localized process. In our 1-year longitudinal MRI and CSF data, the changes in the measures were correlated in the MCI group and the combined use of these markers contributed to improving the diagnostic accuracy for MCI and normal control groups. However, because our study did not yet yield sufficient numbers of decliners we are not able to report on conversion questions.

Another promising avenue for clinical research concerns the dilution or clearance of brain-derived proteins from the CSF. Numerous studies point to abnormal CSF clearance as part of the late-onset AD syndrome. Although there is minimal information regarding age-related and/or AD related changes in CSF turnover, there is ample speculation that reduced clearance could affect the accuracy of the LP measured concentrations of P-tau231 and Aβ4X (which are presumed to reflect the rate of delivery and or egress from the CSF pool) and possibly even influence the course of the neural degeneration. Our recently published results suggest that correction for the dilution of the biomarker in the enlarged CSF pool typically found in AD contributes to detecting longitudinal concentration changes in MCI patients. Clearly additional studies on CSF flow and clearance dynamics are needed.

In conclusion, the combined use of MRI and CSF diagnostic measures for AD have the promise to improve the early and specific diagnosis of AD as well as to improve our understanding of the course of AD on both brain and behaviour. Such information will contribute to improved selection of study subjects in clinical trials and for improved monitoring of treatment effects.

Conflict of interest statement

No conflict of interest was declared.

Acknowledgements

We thank Ms Elissa Thorn and Ms Catherine Cianci for their excellent study coordination. This study was supported by NIH AG12101, AG08051, AG03051, The Silberstein Institute for Aging and Dementia, and the American Health Assistance Foundation.

References

1 Brookmeyer R, Gray S, Kawas C. Projections of Alzheimer's disease in the United States and the public health impact of delaying disease onset. *Am J Public Health* 1998; **88:** 1337–42.
2 The Ronald and Nancy Reagan Research Institute of the Alzheimer's Association and the National Institute on Aging Working Group. Consensus report of the Working Group on molecular and biochemical markers of Alzheimer's disease. *Neurobiol Aging* 1998; **19:** 109–16.
3 Benveniste H, Einstein G, Kim KR, Hulette C, Johnson GA. Detection of neuritic plaques in Alzheimer's disease by magnetic resonance microscopy. *Proc Natl Acad Sci U S A* 1999; **96:** 14079–84.
4 Zhen W, Han H, Anguiano M, Lemere CA, Cho CG, Lansbury PT Jr. Synthesis and amyloid binding properties of rhenium complexes: preliminary progress toward a reagent for SPECT imaging of Alzheimer's disease brain. *J Med Chem* 1999; **42:** 2805–15.
5 Skovronsky DM, Zhang B, Kung MP, Kung HF, Trojanowski JQ, Lee VM. In vivo detection of amyloid plaques in a mouse model of Alzheimer's disease. *Proc Natl Acad Sci U S A* 2000; **97:** 7609–14.
6 Wengenack TM, Curran GL, Poduslo JF. Targeting alzheimer amyloid plaques in vivo. *Nat Biotechnol* 2000; **18:** 868–72.
7 Agdeppa ED, Kepe V, Liu J *et al.* Binding characteristics of radiofluorinated 6-dialkylamino-2-naphthylethylidene derivatives as positron emission tomography imaging probes for beta-amyloid plaques in Alzheimer's disease. *J Neurosci* 2001; **21:** 1–5.
8 Mathis CA, Bacskai BJ, Kajdasz ST *et al.* A lipophilic thioflavin-T derivative for positron emission tomography (PET) imaging of amyloid in brain. *Bioorg Med Chem Lett* 2002; **12:** 295–8.
9 Ball MJ. Topographic distribution of neurofibrillary tangles and granulovascular degeneration in hippocampal cortex of aging and demented patients. A quantitative study. *Acta Neuropathol (Berl)* 1978; **42:** 73–80.
10 Ball MJ, Hachinski V, Fox A *et al.* A new definition of Alzheimer's disease: a hippocampal dementia. *Lancet* January 1985; 14–6.
11 Braak H. On areas of transition between entorhinal allocortex and temporal isocortex in the human brain. Normal

morphology and lamina-specific pathology in Alzheimer's disease. *Acta Neuropathol (Berl)* 1985; **68:** 325–32.
12 Braak H, Braak E. Neuropathological stageing of Alzheimer-related changes. *Acta Neuropathol (Berl)* 1991; **82:** 239–59.
13 Amaral DG, Insausti R. Hippocampal formation. In: Paxinos G, ed. *The Human Nervous System*. San Diego: Academic Press, Inc., 1990; 711–55.
14 Laird NM, Ware JH. Random effects model for longitudinal data. *Biometrics* 1982; **38:** 963–74.
15 Lorente de No R. Studies on the structure of the cerebral cortex. II. Continuation of the study of the ammonic system. *J Psychologie und Neurologie* 1934; **46:** 113–77.
16 Rosene DL, Van Hoesen GW. The hippocampal formation of the primate brain: A review of some comparative aspects of cytoarchitecture and connections. In: Jones EG, Peters A, eds. *Cerebral Cortex*, Vol. 6. New York: Plenum Press, 1987; 345–456.
17 Arnold SE, Hyman BT, Flory J, Damasio AR, Van Hoesen GW. The topographical and neuroanatomical distribution of neurofibrillary tangles and neuritic plaques in the cerebral cortex of patients with Alzheimer's Disease. *Cereb Cortex* 1991; **1:** 103–16.
18 Hyman BT, Van Hoesen GW, Damasio AR, Barnes CL. Alzheimer's disease: cell-specific pathology isolates the hippocampal formation. *Science* 1984; **225:** 1168–70.
19 Hyman BT, Van Hoesen GW, Damasio AR. Memory-related neural systems in Alzheimer's disease: an anatomic study. *Neurology* 1990; **40:** 1721–30.
20 Langui D, Probst A, Ulrich J. Alzheimer's changes in non-demented and demented patients: A statistical approach to their relationships. *Acta Neuropathol* 1995; **89:** 57–62.
21 Hubbard BM, Fenton GW, Anderson JM. A quantitative histological study of early clinical and preclinical Alzheimer's disease. *Neuropathol Appl Neurobiol* 1990; **16:** 111–21.
22 Price JL, Davis PB, Morris JC, White DL. The distribution of tangles, plaques and related immunohistochemical markers in healthy aging and Alzheimer's disease. *Neurobiol Aging* 1991; **12:** 295–312.
23 Arriagada PV, Marzloff K, Hyman BT. Distribution of Alzheimer-type pathologic changes in nondemented elderly individuals matches the pattern in Alzheimer's disease. *Neurology* 1992; **42:** 1681–8.
24 Giannakopoulos P, Hof PR, Mottier S, Michel JP, Bouras C. Neuropathological changes in the cerebral cortex of 1258 cases from a geriatric hospital: retrospective clinicopathological evaluation of a 10-year autopsy population. *Acta Neuropathol (Berl)* 1994; **87:** 456–68.
25 Ulrich J. Alzheimer changes in nondemented patients younger than sixty-five: possible early stages of Alzheimer's disease and senile dementia of Alzheimer type. *Ann Neurol* 1985; **17:** 273–7.
26 Vermersch P, Frigard B, David J-P, Fallet-Bianco C, Delacourte A. Presence of abnormally phosphorylated Tau proteins in the entorhinal cortex of aged non-demented subjects. *Neurosci Lett* 1992; **144:** 143–6.
27 Jellinger KA. Alzheimer's changes in non-demented and demented patients. *Acta Neuropathol (Berl)* 1995; **89:** 112–3.
28 Guillozet AL, Weintraub S, Mash DC, Mesulam MM. Neurofibrillary tangles, amyloid, and memory in aging and mild cognitive impairment. *Arch Neurol* 2003; **60:** 729–36.
29 Giannakopoulos P, Herrmann FR, Bussiere T *et al.* Tangle and neuron numbers, but not amyloid load, predict cognitive status in Alzheimer's disease. *Neurology* 2003; **60:** 1495–500.
30 Morris JC, McKeel DW, Storandt M *et al.* Very mild Alzheimer's disease: informant-based clinical, psychometric, and pathological distinction from normal aging. *Neurology* 1991; **41:** 469–78.
31 Braak H, Braak E. Aspects of cortical destruction in Alzheimer's disease. In: Hyman BT, Duyckaerts C, Christen Y, eds. *Connections, Cognition and Alzheimer's Disease*. Berlin: Springer-Verlag, 1997; 1–16.
32 Hof PR, Giannakopoulos P, Bouras C. The neuropathological changes associated with normal brain aging. *Histol Histopathol* 1996; **11:** 1075–88.
33 Naslund J, Haroutunian V, Mohs R *et al.* Correlation between elevated levels of amyloid beta-peptide in the brain and cognitive decline [see comments]. *JAMA* 2000; **283:** 1571–7.
34 Ball MJ. Neuronal loss, neurofibrillary tangles and granulovacuolar degeneration in the hippocampus with ageing and dementia. *Acta Neuropathol (Berl)* 1977; **37:** 111–8.
35 Davies DC, Horwood N, Isaacs SL, Mann DMA. The effect of age and Alzheimer's disease on pyramidal neuron density in the individual fields of the hippocampal formation. *Acta Neuropathol (Berl)* 1992; **83:** 510–7.
36 Mann DMA, Yates PO, Marcyniuk B. Some morphometric observations on the cerebral cortex and hippocampus in presenile Alzheimer's disease, senile dementia of Alzheimer's type and Down's syndrome in middle age. *J Neurol Sci* 1985: 139–59.
37 Bobinski MJ, Wegiel J, Wisniewski HM *et al.* Neurofibrillary pathology – correlation with hippocampal formation atrophy in Alzheimer disease. *Neurobiol Aging* 1996; **17:** 909–19.
38 Bobinski M, Wegiel J, Tarnawski M *et al.* Relationships between regional neuronal loss and neurofibrillary changes in the hippocampal formation and duration and severity of Alzheimer disease. *J Neuropath Exp Neurol* 1997; **56:** 414–20.
39 de la Monte SM. Quantitation of cerebral atrophy in preclinical and end-stage Alzheimer's disease. *Ann Neurol* 1989; **25:** 450–9.
40 Gomez-Isla T, Price JL, McKeel DW Jr, Morris JC, Growdon JH, Hyman BT. Profound loss of layer II entorhinal cortex neurons occurs in very mild Alzheimer's disease. *J Neurosci* 1996; **16:** 4491–500.
41 Jack CR Jr, Dickson DW, Parisi JE *et al.* Antemortem MRI findings correlate with hippocampal neuropathology in typical aging and dementia. *Neurology* 2002; **58:** 750–7.
42 Bobinski M, de Leon MJ, Wegiel J *et al.* The histological validation of post mortem magnetic resonance imaging-determined hippocampal volume in Alzheimer's disease. *Neuroscience* 2000; **95:** 721–25.
43 Price J, Ko AI, Wade MJ, Tsou SK, McKeel DW, Morris JC. Neuron number in the entorhinal cortex and CA1 in preclinical Alzheimer disease. *Arch Neurol* 2001; **58:** 1395–402.
44 Kril JJ, Patel S, Harding AJ, Halliday GM. Neuron loss from the hippocampus of Alzheimer's disease exceeds extracellular neurofibrillary tangle formation. *Acta Neuropathol (Berl)* 2002; **103:** 370–6.
45 Thal DR, Rub U, Schultz C *et al.* Sequence of Abeta-protein deposition in the human medial temporal lobe. *J Neuropath Exp Neurol* 2000; **59:** 733–48.

46 Hulette CM, Welsh-Bohmer KA, Saunders AM, Mash DC, McIntyre LM. Neuropathological and neuropsychological changes in 'normal' aging: evidence for preclinical Alzheimer disease in cognitively normal individuals. *J Neuropath Exp Neurol* 1998; **57:** 1168–74.
47 Haroutunian V, Perl DP, Purohit DP *et al.* Regional distribution of neuritic plaques in the nondemented elderly and subjects with very mild Alzheimer disease. *Arch Neurol* 1998; **55:** 1185–91.
48 Adlard PA, Vickers JC. Morphologically distinct plaque types differentially affect dendritic structure and organisation in the early and late stages of Alzheimer's disease. *Acta Neuropathol (Berl)* 2002; **10:** 377–83.
49 Ghebremedhin E, Schultz C, Braak E, Braak H. High frequency of apolipoprotein E ε4 allele in young individuals with very mild Alzheimer's disease-related neurofibrillary changes. *Exp Neurol* 1998; **15:** 152–5.
50 Schmechel DE, Saunders AM, Strittmatter WJ *et al.* Increased amyloid eta-peptide deposition in cerebral cortex as a consequence of apolipoprotein E genotype in late-onset Alzheimer disease. *Proc Natl Acad Sci U S A* 1993; **90:** 9649–53.
51 Warzok RW, Kessler C, Apel G *et al.* Apolipoprotein E4 promotes incipient Alzheimer pathology in the elderly. *Alzheimer Dis Assoc Disord* 1998; **12:** 33–9.
52 McNamara MJ, Gomez-Isla T, Hyman BT. Apolipoprotein E genotype and deposits of Abeta40 and Abeta42 in Alzheimer disease. *Arch Neurol* 1998; **55:** 1001–4.
53 Hulstaert F, Blennow K, Ivanoiu A *et al.* Improved discrimination of AD patients using β-amyloid (1–42) and tau levels in CSF. *Neurology* 1999; **52:** 1555–62.
54 Andreasen N, Minthon L, Davidsson P *et al.* Evaluation of CSF-tau and CSF-Abeta42 as diagnostic markers for alzheimer disease in clinical practice. *Arch Neurol* 2001; **58:** 373–9.
55 Green AJ, Harvey RJ, Thompson EJ, Rossor MN. Increased tau in the cerebrospinal fluid of patients with frontotemporal dementia and Alzheimer's disease. *Neurosci Lett* 1999; **259:** 133–5.
56 Riemenschneider M, Buch K, Schmolke M, Kurz A, Guder WG. Cerebrospinal protein tau is elevated in early Alzheimer's disease. *Neurosci Lett* 1996; **212:** 209–11.
57 Vigo-Pelfrey C, Seubert P, Barbour R *et al.* Elevation of microtubule-associated protein tau in the cerebrospinal fluid of patients with Alzheimer's disease. *Neurology* 1995; **45:** 788–93.
58 Arai H, Terajima M, Miura M *et al.* Tau in cerebrospinal fluid: a potential diagnostic marker in Alzheimer's disease. *Ann Neurol* 1995; **38:** 649–52.
59 Kahle PJ, Jakowec M, Teipel SJ *et al.* Combined assessment of tau and neuronal thread protein in Alzheimer's disease CSF. *Neurology* 2000: 1498–504.
60 Skoog I, Vanmechelen E, Andreasson LA *et al.* A population-based study of tau protein and ubiquitin in cerebrospinal fluid in 85-year-olds: relation to severity of dementia and cerebral atrophy, but not to the apolipoprotein E4 allele. *Neurodegeneration* 1995; **4:** 433–42.
61 Motter R, Vigo-Pelfrey C, Kholodenko D *et al.* Reduction of B-Amyloid peptide$_{42}$ in the cerebrospinal fluid of patients with Alzheimer's disease. *Ann Neurol* 1995; **38:** 643–8.
62 Galasko D, Chang L, Motter R *et al.* High cerebrospinal fluid tau and low amyloid beta42 levels in the clinical diagnosis of Alzheimer disease and relation to apolipoprotein E genotype. *Arch Neurol* 1998; **55:** 937–45.
63 Tapiola T, Pirttila T, Mehta PD, Alafuzofff I, Lehtovirta M, Soininen H. Relationship between apoE genotype and CSF beta-amyloid (1–42) and tau in patients with probable and definite Alzheimer's disease. *Neurobiol Aging* 2000; **21:** 735–40.
64 Golombowski S, Muller-Spahn F, Romig H, Mendla K, Hock C. Dependence of cerebrospinal fluid Tau protein levels on apolipoprotein E4 allele frequency in patients with Alzheimer's disease. *Neurosci Lett* 1997; **225:** 213–5.
65 Andreasen N, Minthon L, Vanmechelen E. Cerebrospinal fluid tau and Abeta42 as predictors of development of Alzheimer's disease in patients with mild cognitive impairment. *Neurosci Lett* 1999; **273:** 5–8.
66 Okamura N, Arai H, Maruyama M *et al.* Combined analysis of CSF Tau levels and [(123)I]Iodoamphetamine SPECT in mild cognitive impairment: implications for a novel predictor of Alzheimer's disease. *Am J Psychiatry* 2002; **159:** 474–6.
67 Arai H, Morikawa Y, Higuchi M *et al.* Cerebrospinal fluid tau levels in neurodegenerative diseases with distinct tau-related pathology. *Biochem Biophys Res Commun* 1997; **236:** 262–4.
68 Hesse C, Rosengren L, Andreasen N *et al.* Transient increase in total tau but not phospho-tau in human cerebrospinal fluid after acute stroke. *Neurosci Lett* 2001; **297:** 187–90.
69 Buerger nee BK, Padberg F, Nolde T *et al.* Cerebrospinal fluid tau protein shows a better discrimination in young old (<70 years) than in old old patients with Alzheimer's disease compared with controls. *Neurosci Lett* 1999; **277:** 21–4.
70 Arai H, Ishiguro K, Ohna H *et al.* CSF phosphorylated tau protein and mild cognitive impairment: a prospective study. *Exp Neurol* 2000; **166:** 201–3.
71 Vanmechelen E, Vanderstichele H, Davidsson P *et al.* Quantification of tau phosphorylated at threonine 181 in human cerebrospinal fluid: a sandwich ELISA with a synthetic phosphopeptide for standardization. *Neurosci Lett* 2000; **285:** 49–52.
72 Hu YY, He SS, Wang X *et al.* Levels of nonphosphorylated and phosphorylated tau in cerebrospinal fluid of Alzheimer's disease patients: an ultrasensitive bienzyme-substrate-recycle enzyme-linked immunosorbent assay. *Am J Pathol* 2002; **160:** 1269–78.
73 Buerger K, Teipel SJ, Zinkowski R *et al.* CSF tau protein phosphorylated at threonine 231 correlates with cognitive decline in MCI subjects. *Neurology* 2002; **59:** 627–9.
74 Buerger K, Zinkowski R, Teipel SJ *et al.* Differential diagnosis of Alzheimer Disease with cerebrospinal fluid levels of tau protein phosphorylated at threonine 231. *Arch Neurol* 2002; **59:** 1267–72.
75 Sjogren M, Davidsson P, Tullberg M *et al.* Both total and phosphorylated tau are increased in Alzheimer's disease. *J Neurol Neurosurg Psychiatry* 2001; **70:** 624–30.
76 Ishiguro K, Ohno H, Arai H *et al.* Phosphorylated tau in human cerebrospinal fluid is a diagnostic marker for Alzheimer's disease. *Neurosci Lett* 1999; **270:** 91–4.
77 Parnetti L, Lanari A, Amici S, Gallai V, Vanmechelen E, Hulstaert F, Phospho-Tau International Study Group. CSF phosphorylated tau is a possible marker for discriminating Alzheimer's disease from dementia with Lewy bodies. *Neurol Sci* 2001; **22:** 77–8.
78 Mitchell A, Brindle N. CSF phosphorylated tau – does it constitute an accurate biological test for Alzheimer's disease? *Int J Geriat Psychiatry* 2003; **18:** 407–11.

79 Hardy J, Selkoe DJ. The amyloid hypothesis of Alzheimer's disease: progress and problems on the road to therapeutics. *Science* 2002; **297:** 353–6.

80 Jensen M, Schroder J, Blomberg M *et al.* Cerebrospinal fluid A beta42 is increased early in sporadic Alzheimer's disease and declines with disease progression. *Ann Neurol* 1999; **45:** 504–11.

81 Sjogren M, Minthon L, Davidsson P *et al.* CSF levels of tau, beta-amyloid(1–42) and GAP-43 in frontotemporal dementia, other types of dementia and normal aging. *J Neural Transm* 2000; **107:** 563–79.

82 Tapiola T, Pirttila T, Mikkonen M *et al.* Three-year follow-up of cerebrospinal fluid tau, B-amyloid 42 and 40 concentrations in Alzheimer's disease. *Neurosci Lett* 2000; **280:** 119–22.

83 Pirttila T, Koivisto K, Mehta PD *et al.* Longitudinal study of cerebrospinal fluid amyloid proteins and apolipoprotein E in patients with probable Alzheimer's disease. *Neurosci Lett* 1998; **249:** 21–4.

84 Fukuyama R, Mizuno T, Mori S, Nakajima K, Fushiki S, Yanagisawa K. Age-dependent change in the levels of Abeta40 and Abeta42 in cerebrospinal fluid from control subjects, and a decrease in the ratio of Abeta42 to Abeta40 level in cerebrospinal fluid from Alzheimer's disease patients. *Eur Neurol* 2000: 155–60.

85 Mehta PD, Pirttila T, Mehta SP, Sersen EA, Aisen PS, Wisniewski HM. Plasma and cerebrospinal fluid levels of amyloid beta proteins 1-40 and 1-42 in Alzheimer disease. *Arch Neurol* 2000; **57:** 100–5.

86 Bading JR, Yamada S, Mackic JB *et al.* Brain clearance of Alzheimer's amyloid-beta40 in the squirrel monkey: a SPECT study in a primate model of cerebral amyloid angiopathy. *J Drug Target* 2002; **10:** 359–68.

87 Silverberg GD, Levinthal E, Sullivan EV *et al.* Assessment of low-flow CSF drainage as a treatment for AD: results of a randomized pilot study. *Neurology* 2002; **59:** 1139–45.

88 DeMattos RB, Bales KR, Cummins DJ, Dodart J-C, Paul SM, Holtzman DM. Peripheral anti-Abeta antibody alters CNS and plasma Abeta clearance and decreases brain Abeta burden in a mouse model of Alzheimer's disease. *Proc Natl Acad Sci U S A* 2001; **98:** 8850–5.

89 DeMattos RB, Bales KR, Parsadanian M *et al.* Plaque-associated disruption of CSF and plasma amyloid-beta (Abeta) equilibrium in a mouse model of Alzheimer's disease. *J Neurochem* 2002; **81:** 229–36.

90 Shoji M, Kanai M, Matsubara E *et al.* The levels of cerebrospinal fluid Abeta40 and Abeta42(43) are regulated age-dependently. *Neurobiol Aging* 2001: 209–15.

91 Kanai M, Matsubara E, Isoe K *et al.* Longitudinal study of cerebrospinal fluid levels of tau, A beta1–40, and A beta1–42(43) in Alzheimer's disease: a study in Japan. *Ann Neurol* 1998: 17–26.

92 Kanai M, Shizuka M, Urakami K *et al.* Apolipoprotein E4 accelerates dementia and increases cerebrospinal fluid tau levels in Alzheimer's disease. *Neurosci Lett* 1999; **267:** 65–8.

93 Jagust WJ, Friedland RP, Budinger TF, Koss E, Ober B. Longitudinal studies of regional cerebral metabolism in Alzheimer's disease. *Neurology* 1988; **38:** 909–12.

94 Blomberg M, Jensen M, Basun H, Lannfelt L, Wahlund L-O. Increasing cerebrospinal fluid tau levels in a subgroup of Alzheimer patients with apolipoprotein E allele ε4 during 14 months follow-up. *Neurosci Lett* 1996; **214:** 163–6.

95 Arai H, Terajima M, Miura M *et al.* Effect of genetic risk factors and disease progression on the cerebrospinal fluid tau levels in Alzheimer's disease. *JAGS* 1997; **45:** 1228–31.

96 Sunderland T, Wolozin B, Galasko D *et al.* Longitudinal stability of CSF tau levels in Alzheimer patients. *Biol Psychiatry* 1999; **46:** 750–5.

97 Nishimura T, Takeda M, Nakamura Y *et al.* Basic and clinical studies on the measurement of tau protein in cerebrospinal fluid as a biological marker for Alzheimer's disease and related disorders: multicenter study in Japan. *Methods Find Exp Clin Pharmacol* 1998; **20:** 227–35.

98 Andreasen N, Minthon L, Clarberg A *et al.* Sensitivity, specificity, and stability of CSF-tau in AD in a community-based patient sample. *Neurology* 1999; **53:** 1488–94.

99 de Leon MJ, Segal CY, Tarshis CY *et al.* Longitudinal CSF tau load increases in mild cognitive impairment. *Neurosci Lett* 2002; **33:** 183–6.

100 Reiber H. Dynamics of brain-derived proteins in cerebrospinal fluid. *Clin Chim Acta* 2001; **310:** 173–86.

101 Kuo YM, Kokjohn TA, Watson MD *et al.* Elevated abeta42 in skeletal muscle of Alzheimer disease patients suggests peripheral alterations of abetaPP metabolism. *Am J Pathol* 2000: 797–805.

102 Silverberg GDH. The cerebrospinal fluid production rate is reduced in dementia of the Alzheimer's type. *Neurology* 2001; **57:** 1763–6.

103 Preston SD, Steart PV, Wilkinson A, Nicoll JAR, Weller RO. Capillary and arterial cerebral amyloid angiopathy in Alzheimer's disease: defining the perivascular route for the elimination of amyloid beta from the human brain. *Neuropathol Appl Neurobiol* 2003; **29:** 106–17.

104 Markesbery WR, Carney JM. Oxidative alterations in Alzheimer's disease. *Brain Pathol* 1999; **9:** 133–46.

105 Pratico D, Lee VMY, Trojanowski JQ, Rokach J, Fitzgerald GA. Increased F2-isoprostanes in Alzheimer's disease: evidence for enhanced lipid peroxidation in vivo. *FASEB J* 1998; **12:** 1777–83.

106 Montine TJ, Beal MF, Cudkowicz ME *et al.* Increased CSF F2-isoprostane concentration in probable AD. *Neurology* 1999; **52:** 562–5.

107 Pratico D, Clark CM, Lee VM, Trojanowski JQ, Rokach J, Fitzgerald GA. Increased 8, 12-iso-iPF2alpha-VI in Alzheimer's disease: correlation of a noninvasive index of lipid peroxidation with disease severity. *Ann Neurol* 2000; **48:** 809–12.

108 Pratico D, Clark C, Liun F, Lee V, Trojanowski J. Increase of brain oxidative stress in mild cognitive impairment: a possible predictor of Alzheimer disease. *Arch Neurol* 2002; **59:** 972–6.

109 Wahlund LO, Blennow K. Cerebrospinal fluid biomarkers for disease stage and intensity in cognitively impaired patients. *Neurosci Lett* 2003; **339:** 99–102.

110 de Leon MJ, George AE, Stylopoulos LA, Smith G, Miller DC. Early marker for Alzheimer's disease: the atrophic hippocampus. *Lancet* 1989; **2:** 672–3.

111 de Leon MJ, Golomb J, George AE *et al.* The radiologic prediction of Alzheimer's disease: the atrophic hippocampal formation. *Am J Neuroradiol* 1993; **14:** 897–906.

112 Visser PJ, Scheltens P, Verby FRJ *et al.* Medial temporal lobe atrophy and memory dysfunction as predictors for dementia in subjects with mild cognitive impairment. *J Neurol* 1999; **246:** 477–85.

113 Jack CR Jr, Petersen RC, Xu YC *et al.* Prediction of AD with MRI-based hippocampal volume in mild cognitive impairment. *Neurology* 1999; **52:** 1397–403.
114 Wolf H, Jelic V, Gertz HJ, Nordberg A, Julin P, Wahlund LO. A critical discussion of the role of neuroimaging in mild cognitive impairment. *Acta Neurol Scand Suppl* 2003; **179:** 52–76.
115 Johnson KA, Jones K, Holman BL *et al.* Preclinical prediction of Alzheimer's disease using SPECT. *Neurology* 1998; **50:** 1563–71.
116 de Leon MJ, George AE, Golomb J *et al.* Frequency of hippocampal formation atrophy in normal aging and Alzheimer's disease. *Neurobiol Aging* 1997; **18:** 1–11.
117 Du AT, Schuff N, Amend D *et al.* Magnetic resonance imaging of the entorhinal cortex and hippocampus in mild cognitive impairment and Alzheimer's disease. *J Neurol Neurosurg Psychiatry* 2001; **71:** 441–7.
118 Dickerson BC, Goncharova I, Sullivan MP *et al.* MRI-derived entorhinal and hippocampal atrophy in incipient and very mild Alzheimer's disease. *Neurobiol Aging* 2001; **22:** 747–54.
119 Xu Y, Jack CRJ, O'Brien PC *et al.* Usefulness of MRI measures of entorhinal cortex versus hippocampus in AD. *Neurology* 2000; **54:** 1760–7.
120 Juottonen K, Laakso MP, Insausti R *et al.* Volumes of the entorhinal and perirhinal cortices in Alzheimer's disease. *Neurobiol Aging* 1998; **19:** 15–22.
121 Bobinski M, de Leon MJ, Convit A *et al.* MRI of entorhinal cortex in mild Alzheimer's disease. *Lancet* 1999; **353:** 38–40.
122 Toledo-Morrell L, Goncharova I, Dickerson B, Wilson RS, Bennett DA. From healthy aging to early Alzheimer's disease: in vivo detection of entorhinal cortex atrophy. *Ann NY Acad Sci* 2000; **911:** 240–53.
123 Killiany RJ, Gomez-Isla T, Moss M *et al.* Use of structural magnetic resonance imaging to predict who will get Alzheimer's disease. *Ann Neurol* 2000; **47:** 430–9.
124 de Leon MJ, Convit A, Wolf OT *et al.* Prediction of cognitive decline in normal elderly subjects with 2-[18F]fluoro-2-deoxy-D-glucose/positron-emission tomography (FDG/PET). *Proc Natl Acad Sci U S A* 2001; **98:** 10966–71.
125 Convit A, de Asis J, de Leon MJ, Tarshish C, De Santi S, Rusinek H. Atrophy of the medial occipitotemporal, inferior, and middle temporal gyri in non-demented elderly predict decline to Alzheimer's disease. *Neurobiol Aging* 2000; **21:** 19–26.
126 Pietrini P, Azari NP, Grady CL *et al.* Pattern of cerebral metabolic interactions in a subject with isolated amnesia at risk for Alzheimer's disease: a longitudinal evaluation. *Dementia* 1993; **4:** 94–101.
127 Berent S, Giordani B, Foster N *et al.* Neuropsychological function and cerebral glucose utilization in isolated memory impairment and Alzheimer's disease. *J Psychiat Res* 1999; **33:** 7–16.
128 Arnaiz E, Jelic V, Almkvist O *et al.* Impaired cerebral glucose metabolism and cognitive functioning predict deterioration in mild cognitive impairment. *Neuroreport* 2001; **12:** 851–5.
129 Frisoni GB, Laakso MP, Beltramello A *et al.* Hippocampal and entorhinal cortex atrophy in frontotemporal dementia and Alzheimer's disease. *Neurology* 1999; **52:** 91–100.
130 O'Brien JT, Paling S, Barber R *et al.* Progressive brain atrophy on serial MRI in dementia with Lewy bodies, AD, and vascular dementia. *Neurology* 2001; **56:** 1386–8.
131 Chan D, Fox NC, Jenkins R, Scahill RI, Crum WR, Rossor MN. Rates of global and regional cerebral atrophy in AD and frontotemporal dementia. *Neurology* 2001; **57:** 1756–63.
132 Rusinek H, De Santi S, Frid D *et al.* Serial MRI as a predictor of cognitive decline: a six year longitudinal study of normal aging. *Radiology* 2003; **229:** 691–6.
133 Jack CR, Peterson RC, Xu Y, O'Brien PC, Smith GE, Ivnik RJ. Rates of hippocampal atrophy correlate with change in clinical status in aging and AD. *Neurology* 2000; **55:** 484–9.
134 Duvernoy HM. *The Human Hippocampus: An Atlas of Applied Anatomy*. Munchen: J. F. Bergmann Verlag, 1988; 166 pp.
135 Jack CRJ, Bentley MD, Twomey CK, Zinsmeister AR. MR Imaging-based volume measurements of the hippocampal formation and anterior temporal lobe: validation studies. *Radiology* 1990; **176:** 205–9.
136 Haller J, Botteron K, Brunsden B *et al.* Hippocampal MR volumetry. *SPIE* 1994; **2359:** 660–71.
137 Convit A, McHugh PR, Wolf OT *et al.* MRI volume of the amygdala: a reliable method allowing separation from the hippocampal formation. *Psychiatry Res: Neuroimaging* 1999; **90:** 113–23.
138 Convit A, Wolf OT, de Leon MJ *et al.* Volumetric analysis of the pre-frontal regions: findings in aging and schizophrenia. *Psychiatry Res: Neuroimaging* 2001; **107:** 61–73.
139 Gilbert JG, Levee RF, Catalano FL. A preliminary report on a new memory scale. *Percept Mot Skills* 1968; **27:** 277–8.
140 Wechsler D. *Wechsler Memory Scale–Revised*. San Antonio: Psychological Corporation/Harcourt Brace Javanovich, 1987.
141 Flicker C, Ferris SH, Reisberg B. A two-year longitudinal study of cognitive function in normal aging and Alzheimer's disease. *J Geriat Psychiat Neurol* 1993; **6:** 84–96.
142 Mehta PD, Pirttila T, Patrick BA, Barshatzky M, Mehta SP. Amyloid beta protein 1–40 and 1–42 levels in matched cerebrospinal fluid and plasma from patients with Alzheimer disease. *Neurosci Lett* 2001; **304:** 102–6.
143 Potempska A, Mack K, Mehta P, Kim KS, Miller DL. Quantification of sub-femtomole amounts of Alzheimer amyloid beta peptides. *Amyloid* 1999; **6:** 14–21.
144 Narkiewicz O, de Leon MJ, Convit A *et al.* Dilatation of the lateral part of the transverse fissure of the brain in Alzheimer's disease. *Acta Neurobiol Exp (Warsz)* 1993; **53:** 457–65.
145 Convit A, de Leon MJ, Golomb J *et al.* Hippocampal atrophy in early Alzheimer's disease: anatomic specificity and validation. *Psychiatr Q* 1993; **64:** 371–87.
146 Bobinski M, Wegiel J, Tarnawski M, de Leon MJ, Dziewiatkowski J, Wisniewski HM. Computer-assisted 3D-reconstruction of the hippocampal formation in AD. *J Neuropath Exp Neurol* 1993; **52:** 263.
147 George AE, de Leon MJ, Stylopoulos LA *et al.* CT diagnostic features of Alzheimer disease: importance of the choroidal/hippocampal fissure complex. *Am J Neuroradiol* 1990; **11:** 101–7.
148 Golomb J, de Leon MJ, Kluger A, George AE, Tarshish C, Ferris SH. Hippocampal atrophy in normal aging: an association with recent memory impairment. *Arch Neurol* 1993; **50:** 967–73.
149 Holodny AI, Waxman R, George AE, Golomb J, Rusinek H, de Leon MJ. MRI differential diagnosis of normal pressure hydrocephalus and Alzheimer disease: significance of the parahippocampal fissures. *Am J Neuroradiol* 1998; **19:** 813–9.

150 Convit A, de Leon MJ, Tarshish C *et al.* Specific hippocampal volume reductions in individuals at risk for Alzheimer's disease. *Neurobiol Aging* 1997; **18:** 131–8.
151 De Santi S, de Leon MJ, Rusinek H *et al.* Hippocampal formation glucose metabolism and volume losses in MCI and AD. *Neurobiol Aging* 2001; **22:** 529–39.
152 Golomb J, Kluger A, de Leon MJ *et al.* Hippocampal formation size in normal human aging: a correlate of delayed secondary memory performance. *Learn Mem* 1994; **1:** 45–54.
153 Golomb J, Kluger A, de Leon MJ *et al.* Hippocampal formation size predicts declining memory performance in normal aging. *Neurology* 1996; **47:** 810–3.
154 Freeborough PA, Woods RP, Fox NC. Accurate registration of serial 3D MR brain images and its application to visualizing change in neurodegenerative disorders. *J Comput Assist Tomogr* 1996; **20:** 1012–22.
155 Fox NC, Freeborough PA. Brain atrophy progression measured from registered serial MRI: validation and application to Alzheimer's disease. *J Magn Reson Imaging* 1997; **7:** 1069–75.
156 Rusinek H, Chandra R. Brain tissue volume measurement from magnetic resonance imaging: a phantom study. *Invest Radiol* 1993; **28:** 890–5.

Correspondence: Dr Mony de Leon, Department of Psychiatry, Center for Brain Health, NYU School of Medicine, 560 First Avenue, New York, NY 10016, USA.
(fax: +1 212 263 3270; e-mail: mony.deleon@med.nyu.edu).